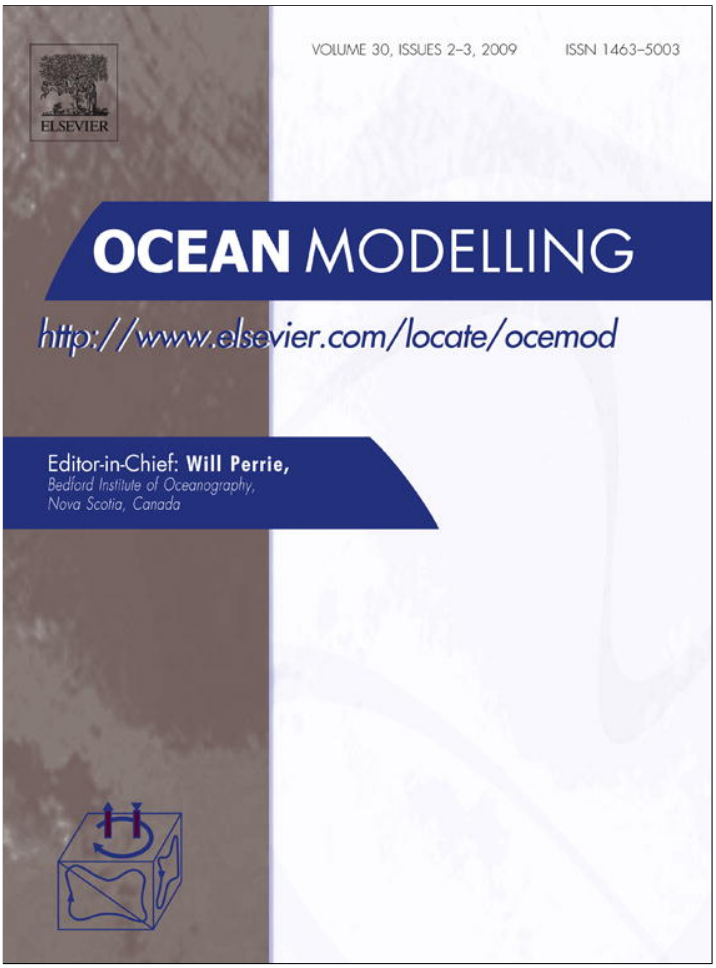

Ocean Modelling 30 (2009) 225–239

Contents lists available at ScienceDirect

Ocean Modelling

journal homepage: www.elsevier.com/locate/ocemod

Investigating the impact of surface wave breaking on modeling the trajectories of drifters in the northern Adriatic Sea during a wind-storm event

Sandro Carniel [a,*], John C. Warner [b], Jacopo Chiggiato [a,c], Mauro Sclavo [a]

[a] Consiglio Nazionale delle Ricerche – ISMAR, Castello 1364, I-30122 Venice, Italy
[b] U.S. Geological Survey, Woodshole, MA, USA
[c] NATO Undersea Research Centre, V.le S. Bartolomeo 400, I-19126 La Spezia, Italy

ARTICLE INFO

Article history:
Received 3 October 2008
Received in revised form 22 June 2009
Accepted 1 July 2009
Available online 21 July 2009

Keywords:
Wave breaking
Turbulence
Drifter

ABSTRACT

An accurate numerical prediction of the oceanic upper layer velocity is a demanding requirement for many applications at sea and is a function of several near-surface processes that need to be incorporated in a numerical model. Among them, we assess the effects of vertical resolution, different vertical mixing parameterization (the so-called Generic Length Scale –GLS– set of k–ε, k–ω, *gen*, and the Mellor–Yamada), and surface roughness values on turbulent kinetic energy (k) injection from breaking waves.

First, we modified the GLS turbulence closure formulation in the Regional Ocean Modeling System (ROMS) to incorporate the surface flux of turbulent kinetic energy due to wave breaking. Then, we applied the model to idealized test cases, exploring the sensitivity to the above mentioned factors. Last, the model was applied to a realistic situation in the Adriatic Sea driven by numerical meteorological forcings and river discharges. In this case, numerical drifters were released during an intense episode of Bora winds that occurred in mid-February 2003, and their trajectories compared to the displacement of satellite-tracked drifters deployed during the ADRIA02-03 sea-truth campaign.

Results indicted that the inclusion of the wave breaking process helps improve the accuracy of the numerical simulations, subject to an increase in the typical value of the surface roughness z_0. Specifically, the best performance was obtained using $\alpha_{CH} = 56{,}000$ in the Charnok formula, the wave breaking parameterization activated, k–ε as the turbulence closure model. With these options, the relative error with respect to the average distance of the drifter was about 25% (5.5 km/day). The most sensitive factors in the model were found to be the value of α_{CH} enhanced with respect to a standard value, followed by the adoption of wave breaking parameterization and the particular turbulence closure model selected.

1. Introduction

Accurate prediction of the surface velocities with a numerical model is a difficult task because of the complicated interplay of several factors affecting the near-surface region. An accurate prediction of the surface velocity in the ocean is required to successfully track the path of a drifting object and has direct relevance for search and rescue operation, littoral activities, and oil-spills emergencies (Reed et al., 1999). When facing the necessity of tracking a generic drifting object, direct observations may not be available to provide details of the spatial and temporal distribution of the driving currents. When they are available, their amount is generally not sufficient, at least not for large areas. This is the reason why we usually rely on surface circulation fields produced by dynamical, state-of-the-art numerical models of the ocean, atmosphere and sea state (Rixen et al., 2007; Carniel et al., 2002; Breivik and Allen, 2008). In order to provide useful products, these fields need to be as accurate as possible.

Typically, the surface layer velocity predictions from numerical models are compared to *in situ* data provided by current meters and high frequency (HF) radar (Breivik and Saetra, 2001). Another accepted way to assess surface layer velocity predictions is to compare the trajectories of "numerical" drifters released during the model integration to the actual paths shown by "real" drifters. With this method, satellite-tracked drifters have recently proved to be a powerful tool (Poulain, 2001) because of the relatively high numbers that can be deployed and because the drifters can be followed for long periods in quasi-real time. Through the efforts of the Dynamics of Localized Currents and Eddy Variability in the Adriatic (DOLCEVITA) project, Ursella et al. (2006) derived the surface circulation at mesoscale to seasonal scale in relation to modeled wind

* Corresponding author. Tel.: +39 329 0845720.
E-mail address: sandro.carniel@ismar.cnr.it (S. Carniel).

1463-5003/$ - see front matter © 2009 Elsevier Ltd. All rights reserved.
doi:10.1016/j.ocemod.2009.07.001

forcing, river runoff, and bottom topography in the Adriatic Sea with unprecedented high horizontal resolution by using more than 120 satellite-tracked drifters.

Barron et al. (2007) evaluated the impact of change in drifter trajectory in the sea surface height assimilating system of a U.S. Navy global model by comparing observed drifters to simulated ones. Using a 3D model during a summer episode of Bora wind (downslope wind from north-east), Beg-Paklar et al. (2008) compared observed and modeled trajectories of two satellite-tacked drifters to determine the forcings imposed on them in different areas of the Adriatic Sea. Haza et al. (2007), using a high-resolution numerical model in the south Adriatic, obtained results that compared well to the location and shape of energetic flow features controlling the near-time fate of drifters.

Drifters have also shown to be useful in integrated approaches, where they helped improving or validating a methodology. Taillandier et al. (2008) used a variational method to reconstruct the velocity field in a portion of the central Adriatic Sea using *in situ* data from nine surface drifters and outputs from a three-dimensional circulation model. Results showed how the reconstruction significantly improved the description of the surface boundary current with respect to the model first guess, capturing its main features and its exchanges with the interior part of the basin when sampled by the drifters. Rixen et al. (2007) also applied a three-dimensional model to the Adriatic Sea to demonstrate hyper-ensemble formulations for predicting surface drifter trajectories. The configuration they used was without the wave breaking option described in this paper but they used the GLS closure (described below) with 30 vertical levels and with a unique value of the Charnok value set at 1400. They showed how it is possible to decrease the degree of uncertainty in reproducing drifters' trajectories when judiciously weighting the outputs from different numerical models using a multi-model ensemble technique to improve predictions towards drifters' trajectories, considered as "the truth". In the latter approach, admittedly, the authors did not attempt to assess the underlying different physics or characteristics of the models, being interested in finding a successful way to "mix" different forecast outputs provided by oceanic numerical models.

However, if we wish to predict surface currents as accurately as possible, it is essential to understand and possibly limit the sources of uncertainty that affect the current fields predicted from numerical models. In this paper we investigate some of the scientific issues that are at the basis of the problem of an accurate numerical simulation of the oceanic upper layer velocity. These issues include the vertical resolution of the surface layer, the choice of vertical mixing schemes and the way it can influence the velocity profile (Mellor and Yamada, 1982; Kantha and Clayson, 1994; Carniel et al., 2007), the effect of surface wave breaking (Jones and Monismith, 2008; Burchard, 2001; Umlauf and Burchard, 2003; Kantha and Clayson, 2004; Kantha, 2006) and the surface roughness parameterization impact on the upper velocity (Stips et al., 2005; Jones and Monismith, 2008). They will be described in Section 2.

We explored these issues by using the Regional Ocean Modeling System (ROMS). ROMS is a three-dimensional, hydrostatic, ocean circulation model that solves the Boussinesq Reynolds Averaged form of the Navier Stokes Equations (Shchepetkin and McWilliams, 2005; Haidvogel et al., 2008). We modified the GLS (Umlauf and Burchard, 2003) turbulence closure that was incorporated by Warner et al. (2005) to include a surface flux of turbulent kinetic energy from breaking waves and to allow options for computation of the surface roughness length, as described in Section 2. Tests were then conducted both on idealized cases presented in Section 3 and in a realistic case in the Adriatic Sea during the 2003 winter period, as discussed in Section 4.

2. Factors affecting modeling predictions of surface layer dynamics

In this paper we focus on some issues that are affecting the prediction of surface velocity, such as the vertical resolution, the mixing scheme for turbulence, the effects of surface wave breaking, and the surface roughness parameterization. Each of these is shortly described below.

2.1. Model vertical resolution

One way to classify oceanic general circulation models is by their vertical coordinate system. The three most commonly used choices for the vertical coordinate are constant elevation (almost equal to pressure, e.g., "z levels"), topography following (fractional distance between the sea bottom and the surface, e.g., "sigma" coordinate models), and density (isopycnic surfaces corrected for the compressibility effect of pressure). For any choice of the vertical coordinate system, typical applications of three-dimensional hydrodynamic models to oceanic environments usually have relatively coarse vertical resolution because oceanic motions are mainly horizontal and because high vertical resolution requires intense computational resources. Therefore the vertical resolution, especially the near surface layers, are not usually discretized with adequate detail.

Since there are advantages and drawbacks associated with the actual choice of the vertical coordinate system, the question of what is the most appropriate choice has not been solved, but for coastal applications the choice of "sigma-coordinate" model is the most popular. In these models the thickness of the upper level is varying from point to point in the x–y domain, according to the water depth; as a consequence, when we change the model vertical resolution, the corresponding modeled "surface" velocities are representative of a different discrete region close to the surface, and this can lead to models reproducing different surface velocities, depending on the local water thickness, as shown by Signell et al. (2002) (where the application of an ocean model to the Adriatic Sea using two different vertical resolutions yielded to higher surface velocities for the increased resolution simulation). A modified version of "sigma-coordinate" that gives more flexibility when defining the vertical layers is represented by the "s-coordinate system" (following Song and Haidvogel, 1994 as modified by Shchepetkin and McWilliams, 2005).

2.2. Vertical mixing

State-of-the-art three-dimensional ocean circulation models compute subgrid scale momentum and tracer mixing by means of second-order closure (SOC) turbulence models. The most common form of a SOC model is a two-equation model where prognostic equations are solved for the turbulent kinetic energy (k) and for a variable related to a length scale (ℓ) (e.g., Mellor and Yamada, 1982; Rodi, 1987). In short, the derivation of these SOC models starts from the Reynolds Averaged Navier–Stokes equations with the turbulent fluxes parameterized in terms of the mean-flow quantities as:

$$\overline{u'w'} = -K_M \frac{\partial U}{\partial z}; \quad \overline{v'w'} = -K_M \frac{\partial V}{\partial z}; \quad \overline{w'\rho'} = -K_H \frac{\partial \rho}{\partial z} \tag{1}$$

where K_M is the eddy viscosity for momentum, K_H is the eddy diffusivity for temperature and salinity, U, V are the mean velocities and u', v', w' are the turbulent components of velocity in the horizontal (x and y) and vertical (z) directions, and ρ and ρ' are total and turbulent components for density.

The dynamical determination of the eddy viscosities and diffusivities can be obtained as:

$$K_M \propto S_M k^{1/2}\ell; \quad K_H \propto S_H k^{1/2}\ell \tag{2}$$

using the dimensionless stability functions, S_M or S_H. These stability functions for momentum or tracers depend on shear and stratification, as proposed by Galperin et al. (1988), Kantha and Clayson (1994), or Canuto et al. (2001). The turbulent quantities k (turbulent kinetic energy) and ℓ (turbulent length scale) must be determined in order to close the set of equations. These quantities are related to the dissipation rate, ε, using the well known cascading relation:

$$\ell = (c_\mu^0)^3 k^{3/2}\varepsilon^{-1} \tag{3}$$

based on the size of the dominant eddies and with the parameter c_μ^0 being a numerical constant that is dependent on the particular stability function. For the Kantha and Clayson (1994) stability functions, $c_\mu^0 = 0.5544$.

The aim of a two-equation SOC model is therefore to compute the two physical quantities k and ℓ. The equation for k (Rodi, 1987) can be directly derived from the equations for the Reynolds stresses neglecting advective terms. Assuming down-the-gradient model for diffusion, the total derivative of k is:

$$\frac{Dk}{Dt} = \frac{\partial}{\partial z}\left(\frac{K_M}{\sigma_k}\frac{\partial k}{\partial z}\right) + P + B - \varepsilon \tag{4}$$

where

$$P = \left(-\overline{u'w'}\frac{\partial U}{\partial z} - \overline{v'w'}\frac{\partial V}{\partial z}\right) = K_M M^2; \quad M^2 = \left(\frac{\partial U}{\partial z}\right)^2 + \left(\frac{\partial V}{\partial z}\right)^2 \tag{5}$$

with M^2 being the rate of production due to the shear, $B = (\beta g\overline{w'\theta'} + \beta_S g\overline{w's'})$ the rate of production/destruction by buoyancy, g is the gravity acceleration, β and β_S are the thermal and haline contraction coefficients, σ_k the constant turbulent Schmidt number for k, θ' and s' are the turbulent components of the temperature and salinity.

Contrary to the computation formulation for k, there exist several methodologies to compute the length scale ℓ. Historically, this has been done by first using simple integral expressions and then moving to more complex differential equations. The methodology has evolved to use a general formulation to transport a generic quantity that algebraically can represent a wide range of existing formulations. The Generic Length Scale (GLS) formulation, as developed by Umlauf and Burchard (2003), transports the generic quantity ψ defined as:

$$\psi = \left(c_\mu^0\right)^p k^m \ell^n \tag{6}$$

The parameters p, m, and n are specified to equate ψ to a turbulent quantity. For example, specifying the parameter set $[p, m, n] = [3.0, 1.5, -1.0]$ equates ψ to dissipation, ε. Alternatively, the specification $[-1.0, 0.5, -1.0]$ equates ψ to a turbulence frequency ω, and the set $[2.0, 1.0, -0.67]$ defines a turbulent formulation we refer to as *gen*, derived by Umlauf and Burchard (2003).

The function ψ is then transported via the formulation:

$$\frac{D\psi}{Dt} = \frac{\partial}{\partial z}\left(\frac{K_M}{\sigma_\psi}\frac{\partial \psi}{\partial z}\right) + \frac{\psi}{k}(c_1 P + c_3 B - c_2 \varepsilon F_{wall}) \tag{7}$$

where c_1 and c_2 are coefficients chosen so as to be consistent with von Kármán's constant and with experimental observations for decaying homogeneous, isotropic turbulence (Wilcox, 1998, pp. 128–131). The parameter c_3 takes on the value of c_3^- in stably stratified flows, and c_3^+ in unstable flows (with additional description provided in Warner et al., 2005). The parameter σ_ψ is the turbulence Schmidt number for ψ and F_{wall} is a wall function. Parameter values are summarized in Table 1 (the F_{wall} term, despite being always 1 for all the cases, has been retained for consistency with the Warner et al. (2005) paper).

Table 1
Complete list of parameters employed when using the Generic Length Scale approach. Values from Burchard and Bolding (2001), Umlauf (pers. comm.), Umlauf and Burchard (2003) and Warner et al. (2005).

	k–ε $\psi = (c_\mu^0)^3 k^{3/2}\ell^{-1}$	k–ω $\psi = (c_\mu^0)^{-1} k^{1/2}\ell^{-1}$	*gen* $\psi = (c_\mu^0)^2 k^1 \ell^{-2/3}$
P	3.0	−1.0	2.0
M	1.5	0.5	1.0
N	−1.0	−1.0	−0.67
σ_k	1.0	2.0	0.8
σ_ψ	1.3	2.0	1.07
C_1	1.44	0.555	1.0
C_2	1.92	0.833	1.22
c_3^+	1.0	1.0	1.0
$k_{\min}$	7.6 e−6	7.6 e−6	7.6 e−6
$\psi_{\min}$	1.0 e−12	1.0 e−12	1.0 e−12
F_{wall}	1.0	1.0	1.0
c_3^-	−0.41	−0.58	0.10

The SOC model is then defined as a combination of the transport of k (4) and the transport of the defined quantity ψ (7). These provide the described SOC models k–ε, k–ω, and k–*gen*. The ε equation is one of the most widely used today, as it pertains to a physically meaningful and rather fundamental property of turbulence. The ω equation, originally proposed by Wilcox (1988), has been noticed lately by geophysical turbulence modelers, and is based on an equation for the turbulence frequency, $\omega \propto k^{1/2}\ell^{-1}$, a physically meaningful quantity involving the length scale. The advantage of the k–ω model is that it can be integrated through the viscous sublayer to the solid wall, without the need for wall functions, making it quite popular in industrial applications. The extension of this model to stratified fluids and the computations of the related empirical parameters, including $c_{\omega 3}$, have been discussed by Umlauf et al. (2003). The formulation for k–*gen* was defined in Umlauf and Burchard (2003) and was based on a set of standard physical constraints to derive a parameter set. There is an active debate on the proper formulation and the physical bases of the GLS formulation (e.g., Kantha and Carniel, 2003); for thorough review works see Umlauf and Burchard (2005) and integrations from Kantha (2006).

2.3. Surface waves breaking

As surface gravity waves travel across the ocean surface, there is a process of wave breaking that produces an injection of turbulent kinetic energy into the upper layer of the ocean. Most of the SOC models above mentioned, however, fail in wave affected surface layers, and viscosity errors translate into unrealistic velocities (Signell et al., 2002; Kantha and Clayson, 2004). When the SOC models were developed they were tuned to treat the sea surface as a solid boundary and therefore, during events of strong wind, reproduce a logarithmic velocity profile in the proximity of the sea surface. On the contrary, the *gen* model of the GLS method imposed a surface breaking formulation in its derivation. For the other methods such as k–ε, k–ω, and MY25 there is a contradiction with recent studies (Craig and Banner, 1994; Craig, 1996; Kantha and Clayson, 2004; Burchard, 2001) and measurements (Terray et al., 1996; Stips et al., 2005) proving that, during breaking wave conditions, the near-surface mixing is higher and the velocity shear lower than those modeled by these non-wave breaking turbulence closure schemes. Indeed the generally accepted view is that there are three dynamical regions near the sea surface (i) an upper layer, completely mixed by wave actions, up to the thickness of one wave height, where high mixing and turbulent kinetic energy dissipation occur; (ii) an intermediate wave-influenced layer of thickness of

several wave heights in which the downward diffusion of k from breaking waves is important and (iii) an outer shear-driven log-layer region.

Recently, mostly in 1D context, two equation turbulence models have successfully been applied accounting for these wave breaking effects (Burchard, 2001; Kantha and Clayson, 2004; Jones and Monismith, 2008). When wave-effects are included, the shear near the surface and the magnitude of the surface currents are reduced. Simulations incorporating wave-enhanced mixing provide a better match to the observed near-surface shear and dissipation rates in 1D situation as shown by Stips et al. (2005), compared to simulations without wave-enhanced mixing. For a more detailed review on the subject, see Jones and Monismith (2008), Kantha (2006) and Umlauf and Burchard (2005).

One way to account for such an effect is to include an additional mixing effect due to breaking of surface gravity waves in the upper ocean, which injects turbulence directly into the upper few meters of the water column. Following recent modeling approaches (Craig and Banner, 1994; Burchard, 2001; Kantha and Clayson, 2004), the surface wave breaking effect can be included by prescribing an additional energy injection in the turbulent kinetic energy and mixing length equations.

We modified the surface boundary conditions in ROMS from that shown in Warner et al. (2005) to include the effects of surface wave breaking and explore how modifications due to wave-enhanced turbulence can affect the modeling of surface velocities. These modifications are similar to the method described by Umlauf and Burchard (2003) and Burchard (2001) and are described in the following.

2.3.1. Boundary conditions for k

We modified the surface flux boundary condition (a.k.a. Von Neumann) for k following Craig (1996), Eq. (7))) as:

$$\left(\frac{K_M}{\sigma_k}\frac{\partial k}{\partial z}\right)\Big|_s = c_w (u_s^*)^3 \tag{8}$$

with u_s^* the friction velocity. The parameter c_w is typically regarded as a function of the sea state with reported values ranging from 50 to 150 (higher values for fully developed seas), and we use a typical value of $c_w = 100$. Without wave breaking, the value is set to $c_w = 0$ to match the previous formulation that was based on a wall log layer.

Using Eq. (4), Craig (1996) derived an analytical solution for k as:

$$k|_s = \frac{(u_s^*)^2}{(c_\mu^0)^2}\left[a + \left(\frac{3\sigma_k}{2}\right)^{1/2} c_\mu^0 c_w \left(\frac{z_0}{z_0 - z}\right)^R\right]^{2/3} \tag{9}$$

where $R = \sqrt{\frac{3}{2}}\frac{c_\mu^0 \sigma_k^{0.5}}{\kappa}$, $\kappa = 0.41$, and $a = 1$ to include shear flows and $a = 0$ for shear free flows, and the second term in the brackets is for shear free turbulence. At the surface $z = 0$ and Eq. (9) was added to provide a Dirichlet surface value for k.

2.3.2. Boundary conditions for ψ

In a similar way, starting from Eq. (6) we can write the vertical derivative for ψ:

$$\left(\frac{K_M}{\sigma_\psi}\frac{\partial \psi}{\partial z}\right) = \frac{K_M}{\sigma_\psi}(c_\mu^0)^p m k^{m-1} \ell^n \frac{\partial k}{\partial z} + \frac{K_M}{\sigma_\psi}(c_\mu^0)^p n k^m \ell^{n-1}\frac{\partial \ell}{\partial z} \tag{10}$$

On the right hand side of Eq. (10), the first term is to allow for a surface flux process and the second term is to match the law of the wall. To include surface wave breaking, Eq. (8) is substituted into the first term on the right hand side of Eq. (10) and the length scale is identified as $\ell = \kappa(z_0 - z)$. These substitutions in Eq. (10) yield

$$\left(\frac{K_M}{\sigma_\psi}\frac{\partial \psi}{\partial z}\right)\Big|_s = -\frac{\sigma_k}{\sigma_\psi}(c_\mu^0)^p m k^{m-1}(\kappa(z_0 - z))^n c_w (u_s^*)^3 - \frac{K_M}{\sigma_\psi}(c_\mu^0)^p n k^m \kappa^n (z_0 - z)^{n-1} \tag{11}$$

Eq. (11) was coded into ROMS to modify the surface flux boundary condition and to allow for wave breaking. The flux is imposed at a location of $z = -0.5\,Hz$, where Hz is the grid cell thickness of the upper layer. If we neglect surface wave breaking ($c_w = 0$), the first term on the rhs vanishes to zero at the surface resulting in the boundary conditions (Warner et al., 2005; see Eq. (54)).

The Dirichlet boundary condition for ψ follows from Eq. (6) $\psi = (c_\mu^0)^p k^m \ell^n$ to yield for inclusion of surface wave breaking:

$$\psi_s = (c_\mu^0)^p k^m (\kappa(z_0 - z))^n \tag{12}$$

Eq. (12) was added to the GLS implementation in ROMS to provide the Dirichlet value at the surface.

Burchard (2001) identified that the vertical diffusion coefficient σ_ψ (the Schmidt number) was determined based on the law of the wall. However, this will yield to incorrect results for some of the SOC models that will not correctly diffuse ψ in shear free turbulence, to which surface wave breaking can be assimilated. To correct this issue, we modified the computation of the diffusion coefficient in ROMS by starting with Eq. (7) for transport of ψ for steady state, unstratified, and uniform horizontal gradients, and using Eqs. (9) for k (with $a = 0$) and (12) for ψ. Combining these equations, one derives the expression:

$$\sigma_\psi = \frac{\kappa^2}{c_2 F_{wall}(c_\mu^0)^2}\left(n^2 - \frac{4}{3}Rnm - \frac{1}{3}Rn + \frac{2}{9}mR^2 + \frac{4}{9}R^2 m^2\right) \tag{13}$$

Eq. (13) is consistent with Eq. (31) of Umlauf and Burchard (2003). This provides a value for σ_ψ where shear production is zero but dissipation is high. We included this parameterization in ROMS to allow the magnitude of σ_ψ to vary vertically as a function of P/ε. At the surface $P/\varepsilon = 0$ and σ_ψ is calculated from Eq. (13). The value of σ_ψ is linearly interpolated to the typical specified value for the closure (Table 1) until a depth is reached where $P/\varepsilon = 1$, computed internally by the model.

2.4. Surface roughness

To close the above formulations, we require the computation of a value for the sea surface roughness, z_0 (also called *surface mixing length*, see Gemmrich and Farmer, 1999). This can be fixed as a user specified value or parameterized. Alternatively, we implemented the computation following Charnok (1955):

$$z_0 = \mathrm{MAX}\left(\frac{\alpha_{CH}}{g}(u_s^*)^2, z_{0\_min}\right) \tag{14}$$

where $\alpha_{CH} = 1400$ is the suggested default value in the absence of breaking waves and z_{0_min} is a user defined minimum surface roughness length. Nevertheless, many authors have debated whether this value should be modified or not when wave breaking is present. Terray et al. (1996) suggested that z_0 should be of the same order as the significant wave height (H_S); Stacey (1999) proposed $z_0 = c_s H_S$, where $c_s = 0.5$. Kantha and Clayson (2004) came up with a fairly consistent value when selecting $z_0 = 1.6 H_S$. Also, Stacey (1999) showed that a higher value of α_{CH}, $O(10^5)$, had to be used in order to have better agreement with his data set, when using a 2D model. Stips et al. (2005) found a better agreement between model and data when using $\alpha_{CH} = 14{,}000$. In a recent paper, Jones and Monismith (2008) used 32,000 as a suitable choice for improving model results. However, none of them were trying to model the surface layer during strong and intense wind events.

Table 2
Specifics adopted in the idealized tests. The combination of these parameters led to a number of 72 runs.

Vertical resolution (m)	SOC models	Charnok parameters	Wave breaking
0.65			
	k–ε	1400	
0.166			*on*
	k–ω	14,000	
0.055			*off*
	gen	56,000	
0.016			

3. Idealized test cases

An idealized test case was set up to explore parameter space of the above mentioned control factors of vertical resolution, SOC models, Charnok values, and surface wave breaking fluxes. The numerical domain consisted of a grid of 7 by 5 points, with a constant grid size of 1000 m. The water depth was set at 50 m. The computational time step was 10 s, and periodic western-eastern boundary conditions were adopted; the Coriolis effect was disregarded. The water dynamics was forced by a wind easterly directed having $u_s^* = 0.01$ m/s (these values were chosen to be consistent with Burchard, 2001). We tested several realizations of the model, with the parameter set as shown in Table 2. Four different vertical resolution configurations were used, using a stretched grid close to the surface region in order to obtain higher resolutions. The number of vertical levels were 16, 30, 80 and 300, to which corresponding maximum resolutions were 0.625, 0.167, 0.0625 and 0.0167 m. Different tests were then performed using three different SOC models (k–ε, k–ω and *gen*), three different values of Charnok constant (1400, 14,000 and 56,000) and including/omitting wave breaking effects, implemented as described in Section 2.3. Overall, this led to 72 runs.

The Charnok constant values were, respectively, the classical value, the one adopted by Stips et al. (2005) and a multiple of the latter, between that proposed by Stacey (1999) and by Jones and Monismith (2008).

3.1. Results

Fig. 1 presents the velocity profiles of several numerical experiments after the model has reached a steady state, determined when the kinetic energy reached a plateau. The left panels present the velocity profiles for runs having a constant value of $\alpha_{CH} = 1400$, but different vertical resolutions, different SOC models and wave breaking (WB) *on*/*off* (WB *on*: continuous lines; WB *off*: dotted lines).

Considering panels (*a*), (*b*) and (*c*), we can see how the upper level velocities are reduced when the wave breaking is present (solid lines). In addition, the surface velocities get larger when the upper level resolution is increased. The magnitude of the velocities converges for simulations with minimum vertical grid spacings (0.0167 and 0.0625, red and blue lines).[1] When adopting a vertical spacing of 0.167 m (green line), the magnitude of the velocities is also very close to the converged value. The simulation with the coarsest resolution (0.625 m, black line) did poorly to resolve the near-surface shear since, as expected, the low-resolution case cannot get as close to the surface as the other schemes. This feature is highlighted either if the wave breaking option is *off* or *on*, but the difference between minimum and maximum velocity is slightly larger in the latter case (see continuous lines, panels (*a*), (*b*) and (*c*)).

Generally speaking, we can also compare results when employing different SOC models. The resulting upper layer velocities do not differ substantially. For example, comparing results for the same vertical resolution (say, the blue lines in panels *a*, *b*, and *c*), the peak surface magnitudes are relatively consistent for all the turbulence closure formulations. The highest values are obtained when using *gen* without wave breaking option activated (panel (*c*), dotted line). For these particular applications (unstratified, constant forcing, no horizontal variability), the choice of the particular second-moment turbulence closure model seems to have only a relatively small impact on the determination of the upper velocity. Overall, we can say then that the most striking difference arises when comparing the profiles obtained with or without wave breaking parameterization. In all the cases the surface velocity decreases when the k injection from breaking waves is switched on. This is in agreement with previous studies (Burchard, 2001) and is due to the fact that, together with an increase in the k, we have an increase in the dissipation rate, resulting in a decreasing shear. This picture is also consistent with the generally accepted view of the processes taking place in the wave affected surface layer.

If we look now at Fig. 1, panels (*d*), (*e*) and (*f*), we can depict how the velocity profiles are affected if we now keep the upper level resolution constant (set to 0.0625 m), and alter the wave breaking parameterization, the value of the Charnok constant and type of SOC model. If we compare again the continuous and dotted lines of each color in each panel, the influence of the wave breaking parameterization appears to be clear, since in all the simulations it entails to a decrease of the upper level velocity. The modification of the current vertical profile for the *gen* scheme (panel *f*) seems to penetrate quite deep into the water column. If we focus on a single panel, say (*d*), we can see how the increase of the Charnok coefficient is now leading to a decrease of the upper level velocity as well. This is due to the fact that, by increasing the value of α_{CH}, we are enhancing the surface roughness which leads to an increasing flux of turbulence that enhances the eddy viscosity, creating more mixing and reducing the shear.

It is interesting to highlight the decrease in percentage between maximum/minimum surface velocity for the three different SOC models employed [k–ε, k–ω, *gen*] (see Fig. 1, panels *a*–*c*); for the WB *on* case this was [−7.7, −7.7, −11.1]%, while for WB *off*, ratio values become [−6.9, −10.0, −9.7]%. In Fig. 1 panels (*d*–*f*), the percentage variations are even larger: when WB *on* [−23.3, −20.7, −23.3]%, when WB *off* [−18.7, −18.2, −17.6]%. Therefore, the modification of the Charnok coefficient leads to a larger variation in the upper velocities with respect to what happens when we modify the vertical resolution.

It is also interesting to explore what is the variability of the velocity magnitude when varying WB *on* and *off*, and keeping the vertical resolution constant at different α_{CH} [1400, 14,000, 56,000]. The ratio of the surface velocities for the cases WB *on*/WB *off* are [0.94, 0.91, 0.87] for panel (*d*), [0.89, 088, 0.87] for panel (*e*) and [0.89, 0.88, 0.83] for panel (*f*). When we keep the vertical resolution constant, the decrease in the surface velocity due to the WB parameterization is therefore approximately about 10%, and it is increases with the increase of the Charnok coefficient (1400, 14,000, 56,000). This is valid throughout the water column, except in a single case, panel (*d, blue line*), where there is a small region around 1 m depth where the velocity WB *on* is greater than that modeled using *WB off*.

In order to complement the presentation of results using the GLS scheme as *gen* with wave breaking *on*, in Fig. 2 we present also the profile of k. The injection of surface k due to breaking waves is clearly visible (see Fig. 2, left panel, where all the results have been obtained using a constant $\alpha_{CH} = 1400$), the case *WB off* being characterized by a straight vertical line, representing a constant TKE indicative of the law-of-the-wall behavior.

[1] For interpretation of color mentioned in this test the reader is referred to the web version of the article.

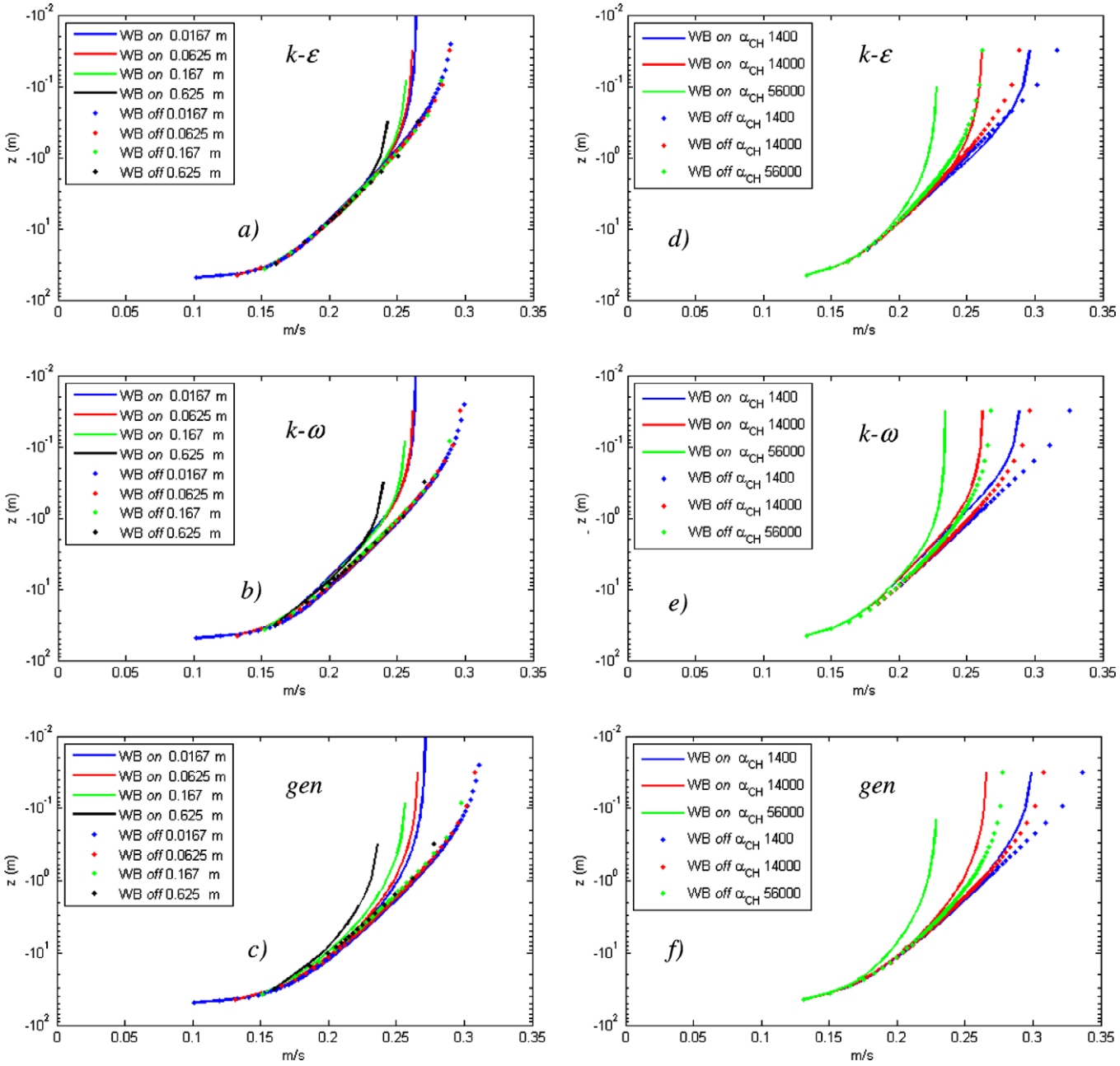

Fig. 1. Currents vertical profiles (m/s) obtained from the idealized experiment. Left panels, from top to bottom: different cases when using a constant $\alpha_{CH} = 1400$ and k–ε (top), k–ω (central) and k–*gen* (bottom). Right panels: the same SOC models cases, but now keeping the vertical resolution constant (0.065 m).

The more we increase the upper level vertical resolution, the more detailed appears to be the slope of the k profile and the lower is the integral value of the k itself, while the maximum surface values remains the same, in agreement with the upper boundary condition imposed.

On the other hand, if we focus on a single case as in the right panel of Fig. 2 (i.e., constant vertical resolution 0.0625 m, again *gen*) and we vary the WB *on*/*off* or the Charnok constant, we see again that the WB *off* option is yielding a straight profile, while the increase in the Charnok value leads to an increase of the integral value of the k. Overall, while there is an inverse proportionality between the increase in the vertical resolution and the integral value of turbulent kinetic energy, there is a direct proportionality between the increase of the Charnok value and the average integral value of k.

Fig. 3 shows the eddy viscosity (m^2/s) as corresponding to the idealized experiment, again using GLS as *gen*. The left panel shows the different cases with a constant $\alpha_{CH} = 1400$. The shapes of the diffusivities when using the WB *off* almost overlap, while when using WB *on* the shape becomes more and more parabolic when we increase the vertical resolution. In the right panel we show different cases of what happens when using a constant vertical resolution (0.0625 m) at different Charnok parameters. As expected, the increase in the α_{CH} leads to a higher level of diffusivity, also at the surface.

4. Application to the Adriatic Sea

To further address the issues of SOC models, Charnok values, and surface wave breaking fluxes, the modeling system was ap-

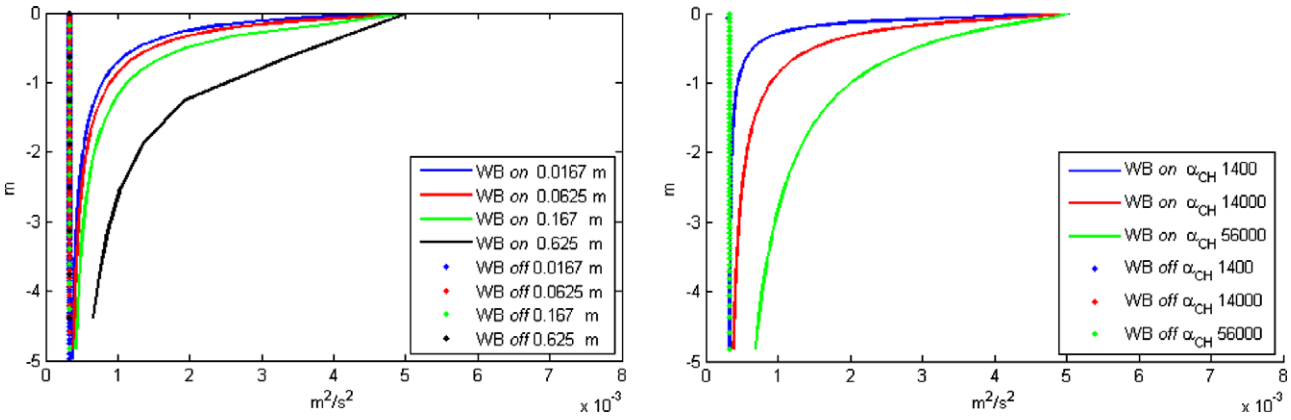

Fig. 2. Turbulent kinetic energy (m^2/s^2) from the idealized experiment, using GLS as *gen*. Left: different vertical resolution, but constant $\alpha_{CH} = 1400$; right: different cases when using a constant vertical resolution (0.065 m).

plied to a realistic situation in the northern Adriatic Sea. Results are discussed here with particular focus on the upper layer velocities and shears in the basin. The model results have been indirectly validated by comparing the trajectories of virtual floaters against those of real drifters. This is a very demanding task since many features are involved in determining the trajectory of a drifter (Beg-Paklar et al., 2008).

Between September 2002 and March 2003, the international scientific program ADRIA02-03 was carried out under the supervision of the NATO Undersea Research Centre (NURC, La Spezia, Italy), and the R/V *Alliance* sampled the northern/central Adriatic waters by means of CTD and hydrologic measurements (see for example, Sherwood et al., 2004; Martin et al., 2006). During the cruises, in the framework of the DOLCEVITA project (Lee et al., 2005), more than 60 drifters were deployed in the basin, subject to different meteorological conditions, and most of them were successfully satellite tracked (Ursella et al., 2006; Taillandier et al., 2008). Drifters were of the CODE type, equipped with a Global Positioning System (GPS), programmed to sample position at 1 h intervals; data were kept in memory on the drifter before being transmitted to Argos satellite system. Direct measurements studies showed that the CODE drifters can be considered efficient instruments to measure the surface velocity current in the first meter of the water column with 1–2 cm/s accuracy (Poulain et al., 2009). More details on the drifter positions, tracks and density can be found in Ursella et al. (2006).

The numerical grid used in this realistic application was curvilinear and consisted of 160 × 60 grid points, accounting for a maximum horizontal resolution of roughly 2.5 × 2.5 km, with mean resolution of 5 × 4 km. Along the vertical, either 30 or 80 s-coordinate levels were used. The model was initialized at rest by means of the hydrological data collected during the field trial in September 2002. Advection for momentum was discretized with a third-order upstream scheme (Shchepetkin and McWilliams, 1998), while for tracers we used an MPDATA family scheme (Margolin and Smolarkiewicz, 1998) together with a weak grid-size dependent diffusivity. A density based Jacobian with spline reconstruction of vertical profiles was used for the representation of the pressure gradient term (Shchepetkin and McWilliams, 2003). The numerical scheme adopted for the vertical mixing was based on the GLS approach proposed by Warner et al. (2005) and the modifications suggested above for the surface wave breaking option when included. The surface forcings (wind speed and direction at 10 m, atmospheric pressure, air and dew temperature at 2 m, total cloud cover, net short wave radiation) during the period of the simulation were received from the high-resolution limited-area model LAMI (Italian implementation of the non-hydrostatic model LM, Steppeler et al., 2003) run by the HydroMeteorological Service of Emilia Romagna Region (ARPA-SIMC), Italy. Products were available in the whole Adriatic basin at 3 h time intervals, with a spatial resolution of about 7 km. Net long wave (using Berliand formula, Budyko, 1974), latent, sensible and momentum flux using Fairall et al. (2003), were computed internally by ROMS using its own sea surface temperature. River inputs were also included in terms of flux of momentum, temperature and salinity. For the Po river, which is the most relevant in terms of flow, direct measurements

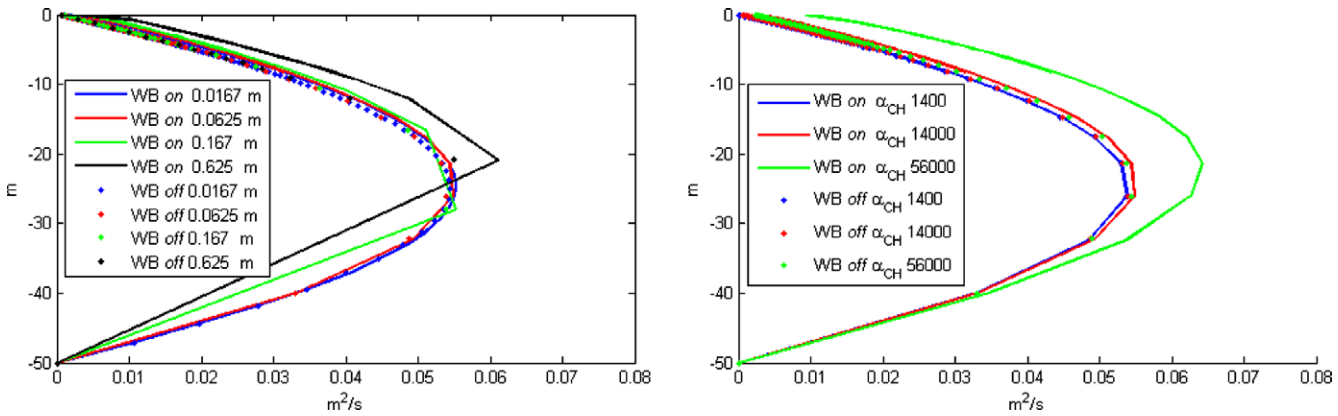

Fig. 3. Eddy viscosity (m^2/s) from the idealized experiment, using GLS as *gen*. Left, different vertical resolution, but constant $\alpha_{CH} = 1400$; right, different cases when using a constant vertical resolution (0.065 m).

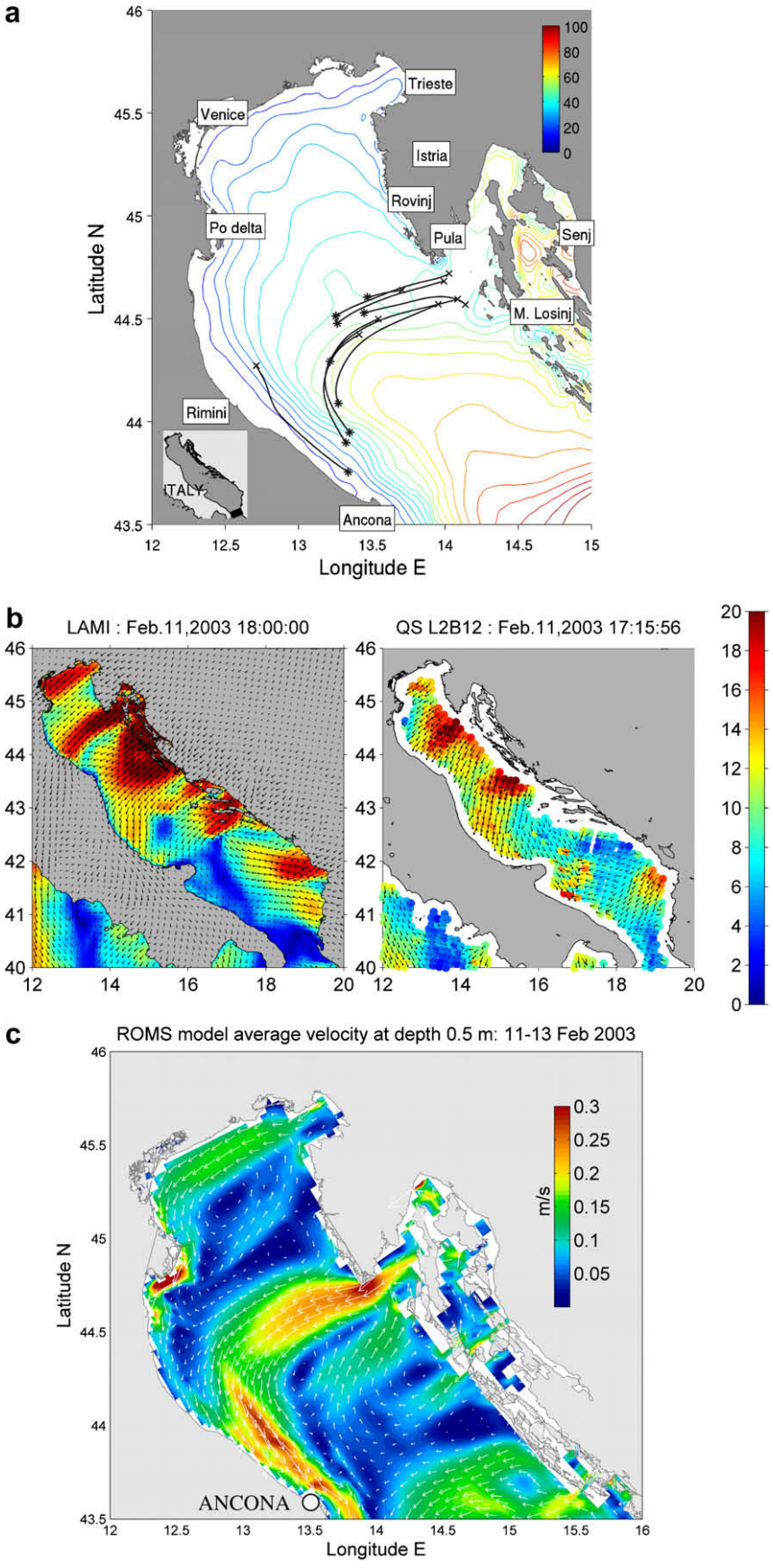

Fig. 4. (a) Contours of North Adriatic Sea bathymetry (color scale) with shown nine out of the fourteen drifters released during the time window 9–14 February, 2003. The insert in the lower left corner presents the numerical grid. (b) Snapshot of the Bora wind field (color bar in m/s) from the model LAMI (left panel) and QuikSCAT L2B12 (courtesy of SeaWinds/QuikSCAT Science Team, JPL, NASA) at nearly corresponding time (UTC). (c) ROMS model average surface velocity (m/s) during the period 11–13 February 2003.

were available. For the remaining 47 rivers, climatological values have been used. On the southern boundary, near Otranto strait (see Fig. 4a, inner panel on left-bottom corner), tides from a finite-element model of the Adriatic Sea (Cushman-Roisin and Naimie, 2002) were applied along with radiation condition for 3D momentum and tracers.

Simulations were performed to test the drifter performance due to variations of surface roughness, SOC, and the effect of including surface wave breaking. To test the surface roughness, we performed the simulations using three different values for Charnok coefficients (1400, 14,000 and 56,000); in addition, we also tested the parameterization $z_0 = aH_S$ (Stacey, 1999). With the latter choice values of significant wave height are computed via the third generation wave model SWAN (Booij et al., 1999), run with the same forcing and on the same grid as ROMS. Four different type of SOC models have been employed. These include the GLS formulation as *gen*, k–ε, k–ω, and the Mellor–Yamada Level 2.5 (Mellor and Yamada, 1982, hereinafter MY2.5) closure, the latter run without surface wave breaking option. The MY2.5 was included because it is widely used and provides a benchmark of a "standard" performance. Floaters trajectories were tested by including and neglecting the surface injection of turbulent kinetic energy due to breaking waves. Table 3 lists all the options of the numerical experiments carried out.

Results presented here refer to the numerical simulation of floaters during an intense Bora episode in the period February 11–13, 2003. Bora wind is a north-easterly downslope wind critically affected by the complex orography surrounding the Adriatic Sea, thus being characterized by a strong spatial variability. Ursella et al. (2006) analyzed the same LAMI wind fields adopted in this study but for a longer period (from 1 September 2002 to 31 December 2003), and showed that the northern Adriatic was characterized by two dominant wind regimes: the north-easterly bora wind and the south-easterly scirocco (occurring with relative frequency of, respectively, 35% and 21%, with no-wind up to 26%, mistral at 10% and libeccio at 8%).

An example of the wind field over the Adriatic basin is presented in Fig. 4b. The use of high-resolution meteorological models helps to have fairly good representation of Bora wind jets (Signell et al., 2005) although even a sub-kilometer resolution of the meteorological model may be required (Askari et al., 2003) and this is crucial for the simulated wind-driven circulation underneath. In fact, the wind curl associated to the series of Bora jets and wakes along the major axis of the Adriatic Sea triggers a complex mesoscale ocean circulation composed by cyclones and anticyclones in the northern-mid Adriatic (Orlić et al., 1994; Kuzmić et al., 2006; Martin et al., 2006; Pullen et al., 2007), and reinforces the Western Adriatic coastal Current (WAC, see Ursella et al., 2006); thus, simulating the correct tracks of drifting objects under such wind storms is a surely challenging problem. For additional details on Bora wind events during February 2003 see Dorman et al. (2006).

Table 3
Specifics adopted in the Adriatic Sea tests. The combination of these parameters led to a number of 48 runs. In addition, two runs with MY2.5 were carried out (for a total of 50 numerical experiments).

SOC models	Surface roughness	Levels	Wave breaking
	1400		
k–ε			
	14,000	30	*on*
k–ω			
	56,000	80	*off*
gen			
	0.5 H_S		
MY2.5	n.a.	30	n.a.
		80	

Being the northern Adriatic a shallow basin (not deeper than 50 m) where during wintertime Bora events the circulation is substantially wind driven, the correct representation of surface currents is clearly strongly dependent on the modeled winds that are feeding the hydrodynamical model. In addition, when reproducing the paths of real drifters, deviations from reality are to be expected for several other reasons. The observed drifters are affected by small-scale processes and structures that are obviously still missing in routinely applied oceanographic models, which are missing some fine spatial variability. In the numerical tests carried out, the drifters were kept in the proximity of the surface (0.5 m below the varying sea surface elevation) by an appropriate routine within the ROMS code.

Fig. 4c depicts the ROMS model average surface velocity during the period 11–13 February 2003; within the simulated period, the model response to the bora events shows evidence of a large cyclonic gyre in the northern Adriatic, together with a smaller anti-cyclonic gyre near the Istrian peninsula. Moving south, while the WAC appears to be evident all along the Italian coast, north of Ancona a substantial part of its flow tends to recirculate towards the Croatian region, forming another cyclone. These patterns were described also by Martin et al. (2006) during a bora episode, although they are referring to a different period of the same year (January i.o. February) and adopting wind fields resulting from a different meteorological model. In the same paper the authors demonstrated how these patterns and their intensity were generally in agreement with ADCP observations obtained in the region during winter 2003, raising the point that, during intense period of winds, the classical picture of the surface circulation in the northern Adriatic basin can be complicated by the existence of smaller structures, albeit transient. Nevertheless, these can directly affect the drifters' trajectory. For further considerations about the Adriatic dynamics reproduced by the same model configuration employed in this paper, refer also to Bignami et al. (2007).

4.1. Results

In the following discussion we focus on the trajectories of drifters in the period 11 February 00 UTC to 13 February 00 UTC, 2003 (please note, however, that the drifters were actually deployed on 9 February).

Five of the simulated drifters are advected into a region with strong currents characterized by a high ratio Eddy Kinetic Energy/Mean Kinetic Energy, i.e., indicating large fluctuations with respect to the mean flow values, at least during Bora events (see Fig. 13, Ursella et al., 2006). It is interesting to point out how, slightly to the north, a region of steady water pools is identified. For these reasons, these drifters are not considered further. Indeed, during the winter period of 2003 (identified as JFM), the analysis of released drifters to the south of the tip of Istria presented by Ursella et al. (2006) depicted the following prominent features: a strong WAC along the Italian coast, a vigorous cyclone in the northern Adriatic region and a strong recirculation pattern (i.e., another cyclone south of the northern Adriatic) in the south of Istria.

Following Kundu (1976), we assessed how many among the remaining drifters were found to follow a free, almost directly wind-driven flow, by computing the average veering between the drifter and the wind (as obtained by the LAMI meteorological model) velocity directions. As a result, the behavior of six drifters could be assimilated as being under direct influence of wind (roughly, veering 15–20° to the right of the wind), while three are clearly non-wind driven. It should be pointed out that, being the procedure adopted based on averaged areas and velocities, there might well be situations where this classification is not sharp (for instance, for drifters that experience different wind situations during their life).

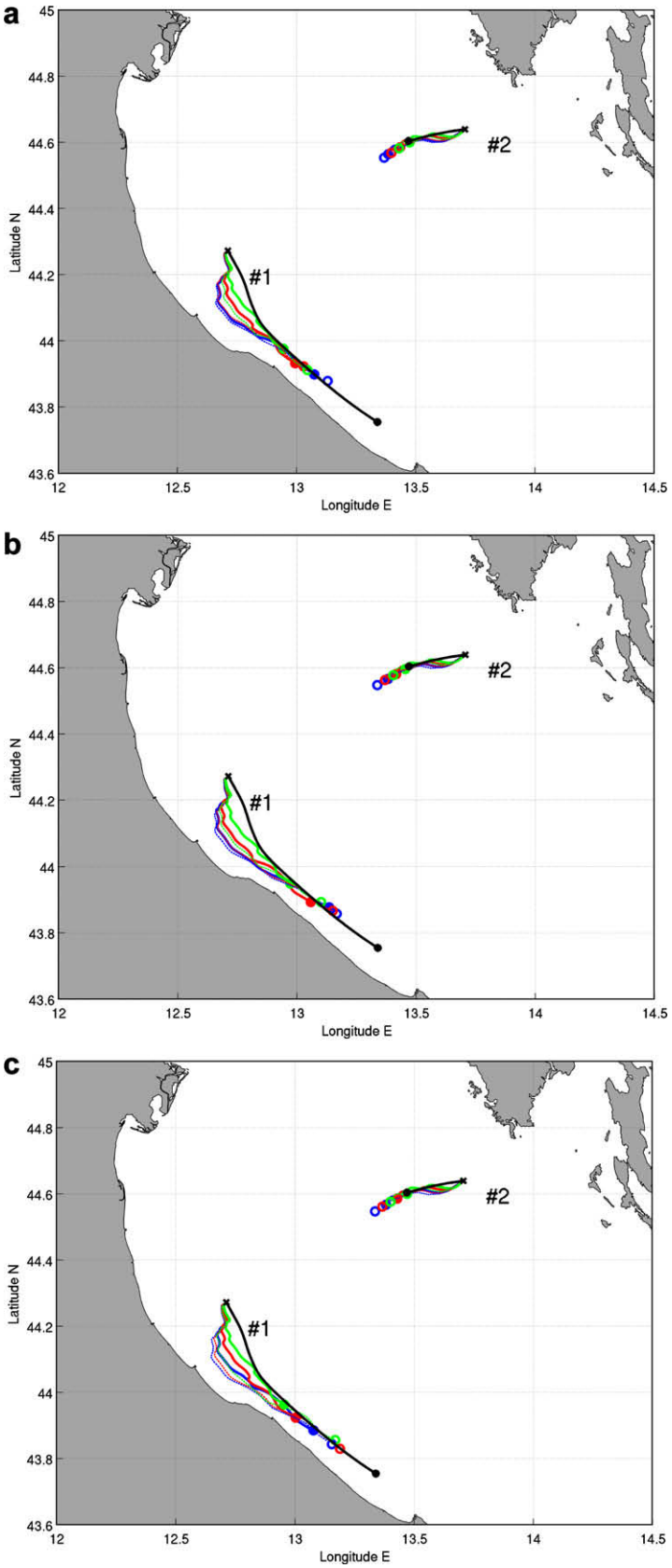

Fig. 5. Trajectories of Drifters #1 and #2 simulated using k–ε (5a, top panel), k–ω (5b, central panel), *gen* (5c, bottom panel). Drifter #1 is traveling in a non-wind-driven region, trapped in the western area of the Adriatic Sea and caught into the Western Adriatic Current (WAC) system. Drifter #2 is under the direct influence of winds, released close to the Croatian coast in a region where wind model results were reliable. The thick black line represents the actual trajectory measured by the GPS tracked floaters, while the thick, full-circle ended (dotted, empty-circled) lines represent results when the wave breaking option is *on* (*off*). The different colors represent different Charnok coefficients, green (α_{CH} = 1400), red (α_{CH} = 14,000) and blue (α_{CH} = 56,000).

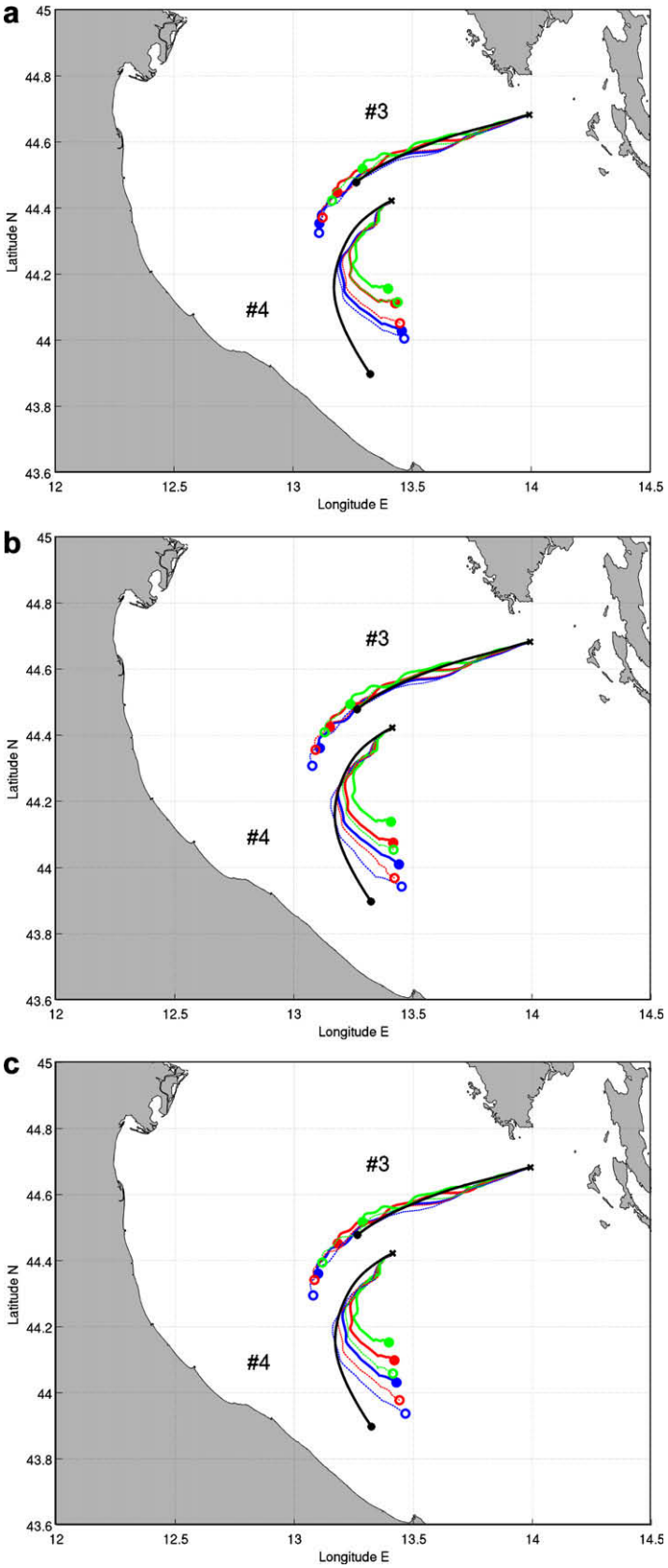

Fig. 6. Trajectories of Drifters #3 and #4 simulated using k–ε (a, top panel), k–ω (b, central panel), *gen* (c, bottom panel). Drifter #3 is under the direct influence of winds, released close to the Croatian coast in a region where wind model results were reliable. Drifter #4 is released in the central part of the basin under the effect of the Bora winds, and quickly deflects towards the WAC region without being trapped into it, therefore experiencing a "mixed" situation. The thick black line represents the actual trajectory measured by the GPS tracked floaters, while the thick, full-circle ended (dotted, empty-circled) lines represent results when the wave breaking option is *on* (*off*). The different colors represent different Charnok coefficients, green (α_{CH} = 1400), red (α_{CH} = 14,000) and blue (α_{CH} = 56,000).

Table 4
Scores (km/day) from experiments grouped by different GLS SOC models (CI−, lower confidence interval; CI+, upper confidence limit).

SOC models	Median	CI−	CI+
k–ε	6.7	6.6	6.8
k–ω	7.4	7.2	7.5
gen	7.5	7.3	7.6

Table 5
Scores (km/day) from experiments grouped by surface roughness parameterization.

Surface roughness	Median	CI−	CI+
α_{CH} = 1400	8.4	8.2	8.5
α_{CH} = 14,000	7.0	6.8	7.2
α_{CH} = 56,000	6.1	6.0	6.3
$z_0 = 0.5\ H_S$	6.7	6.6	6.9

Here we restrict ourselves to a detailed discussion on only four out of the nine drifters, the decision being motivated by the fact that they can be considered representative of "typical" trajectories of the whole remaining series (see Figs. 5 and 6). Drifter #1 was chosen among those traveling in the non-wind-driven region, emblematic of the behavior of floaters released and trapped in the western area of the Adriatic Sea, that are caught into the Western Adriatic Current (WAC) system. Drifters #2 and #3 were chosen among those under the direct influence of winds, representing good examples of drifters released close to the Croatian coast but still in a region where wind model results were reliable. Lastly, Drifter #4 represents a drifter released in the central part of the basin that, under the effect of the Bora winds, is pushed towards the WAC region without being trapped into it, therefore experiencing a "mixed" situation. Moreover, although the strength and width of the WAC as reproduced by the ROMS model (see again Fig. 4c) is in good agreement with previous studies (e.g., Martin et al., 2006; Kuzmić et al., 2006), it has to be noticed that in this region the coastal current structure is deflected towards the Croatian coast, originating a cyclonic eddy. The numerical drifter is released very close to the centre of the eddy and, after being embedded into this gyre, slowly turns its path against the wind and progressively differs from the position of the real one, that is apparently drawn into the WAC more directly (see Fig. 6). Although Drifter #4 is not fully experiencing a direct influence of the wind during its surface dynamics, we considered it as an interesting situation that can be rather often experienced when facing real applications.

Fig. 5(a–c) presents the tracks of Drifters #1 and #2 for, respectively, the three different SOC employed: k–ε, k–ω and *gen*. The thick black line represents the actual trajectory measured by the GPS tracked floaters, while the thick, full-circle ended (dotted, empty-circled) lines represent results when the wave breaking option is *on* (*off*). The different colors represent different Charnok coefficients, green (α_{CH} = 1400), red (α_{CH} = 14,000) and blue (α_{CH} = 56,000). Generally speaking, Drifter #1 trajectories are reproduced to a good level of approximation by all the presented configurations. However, all of the simulated drifters are underestimating the final distance. All the numerical reproduced trajectories are departing from the actual path shortly after the beginning of integration, with the α_{CH} = 14,000, WB *off* cases departing the least.

Table 6
Scores (km/day) from experiments grouped by wave breaking (*on*/*off*).

WB	Median	CI−	CI+
on	6.4	6.3	6.5
off	7.6	7.5	7.7

Table 7
Scores (km/day) from experiments divided by SOC models with basic configuration (WB *off*, α_{CH} = 1400) and MY2.5.

TCM	Median	CI−	CI+
k–ε	7.6	7.5	7.8
k–ω	8.5	8.3	8.8
gen	8.7	8.5	8.9
MY2.5	10.7	10.2	11.0

Drifter #2 trajectory is also predicted rather well by the simulations; those simulations with wave breaking option *off* (empty circles) all overshoot the final observed locations, while among the other simulations, the one using α_{CH} = 56,000 (green line) ends up in the exact observed location, regardless of the SOC version that is employed. In this case too, the choice of the Charnok parameter has more influence than that of the SOC model adopted or the use of wave breaking.

Fig. 6(a–c) presents Drifters #3 and #4 behavior. The trajectory of the former appears to be nicely reproduced by all the simulations, but only the one using the wave breaking *on* and α_{CH} = 56,000 is not over-estimating the distance. Again, the difference in SOC models appears to be negligible, with the k–ω being the closest by a small margin, while the most relevant parameter is again the value of the Charnok coefficient.

As expected from the above considerations, results from Drifter #4 exhibit the highest degree of scattering. Rather than following the southeastward WAC flow along the Italian coast, the numerical drifters are caught into a recirculation region that pushes them back to the Croatian coasts, and the simulated trajectories are not accurately reproducing the final observed locations. While results from *gen* (Fig. 6b) and k–ω (Fig. 6c) simulations display very similar paths, the k–ε simulation results (Fig. 6a) differ more. The main differences in the resulting trajectories are due to the choice of the Charnok coefficient; the higher the value we employ (green lines), the more the currents slow down. This helps when the simulated drifters overshoot the real ones (as for the case of Drifter #3, see Fig. 6), but does not in opposite circumstances (see Drifter #1, Fig. 5) and cannot compensate in case of clearly biased dynamics (see Drifter #4, Fig. 6).

Generally speaking, including wave breaking leads to improved results in the simulations and this is particularly true for the drifters under the direct influence of the wind (Drifters #2 and #3). There is no doubt, however, that the simulations are more sensitive to the choice of Charnok coefficient (or, equivalently, to the z_0 one) than to the inclusion of wave breaking, and that the choice of the SOC model seems to play a minor role.

4.2. Statistical assessment

Until now we have described qualitatively the most relevant results but, in order to better evaluate the performance of the different experiments, an approach based on statistical scores is desirable. As we briefly mentioned above and outlined in Table 3, for the realistic application in the Adriatic Sea a total of 50 runs were carried out. Following a statistical approach, during the period from 11 February 00 UTC to 13 February 00 UTC, clusters of nine numerical drifters were released every hour, with their initial positions corresponding to the actual drifters' positions at that moment. This corresponded to the release of some 400 virtual drifters for each run.

For each modelled drifter, the distance is estimated from the corresponding observations after 1 day (Ozgokmen et al., 2001; Castellari et al., 2001). Then, the median is selected as a measure of central tendency of the ensemble of errors. Upper/lower confidence intervals for the medians are estimated using a bootstrapping technique with 1000 re-samples (Zoubir, 1993).

The best score (difference between modeled and real drifter of 5.5 km/day) is associated with the run using k–ε, α_{CH} = 56,000, WB *on* (regardless of the vertical levels being 30 or 80, the differences not being statistically relevant); the worst situation is reproduced by the run adopting *gen*, α = 1400, WB *off* and 30 levels (9.3 km/day). MY2.5 with 30 vertical levels is the bottom reference, with 10.7 km/day. However, this scheme was tested only because of its wide popularity mostly in the eighties, and was not subjected, by definition, to the sensitivity and improvements discussed above and related to surface roughness or wave breaking issues. The average distance covered by real drifters is 20.7 km/day, so the range of errors is from roughly 25% to 50% of the total covered distance.

To allow a better synthesis of information, in Table 4–7 we present results obtained by grouping runs on the basis of the selected scheme/configuration. For instance, in Table 4 experiments are grouped by different SOC models, thus disregarding particular surface roughness parameterization, wave breaking option, and so on (in this table MY2.5 is not considered). It can be noticed that k–ε gives lower values, different from the other two schemes; however, the difference is roughly 1 km/day, which is 5% of the average path of the drifters. If we group experiments by the surface roughness parameterization (Table 5), when choosing α_{CH} = 56,000 the score is maximum. The difference between the best and the worst score is 2.5 km/day, corresponding to 12.5% of the average distance. Using $z_0 = 0.5\, H_S$ gives a performance almost comparable to that obtained when using α_{CH} = 56,000; this is not surprising since the two formulations give indeed comparable values for z_0 in this application. Including the wave breaking option seems to be helpful too (see Table 6), resulting in a 1 km/day impact (comparable therefore to the effect evidenced by employing different SOC models, about 5%). The two tested vertical resolutions were chosen in a way that the layer thickness in the region of the drifters' deployment were comparable with those adopted in the test case (N = 30, close to 0.17 m; for N = 80, close to 0.0625 m). In this particular example, the number of vertical levels gives results that are not statistically different in a significant way. Finally, Table 7 shows that even when MY2.5 is compared to GLS schemes with similar configuration (α_{CH} = 1400, wave breaking *off*) it gives scores 2–3 km/day larger.

In conclusion, the statistical assessment shows that the model performances are affected to a larger degree by the use of different surface roughness values, and only to a lesser degree to the inclusion of wave breaking or the choice of the SOC model.

5. Conclusions and recommendations

In this paper we mainly address some of the aspects related to the determination of the most accurate surface velocity resulting from oceanic numerical models. By carrying out idealized and realistic test cases, we assess what is the most significant factor among model vertical resolution, different state-of-the-art SOC models, inclusion of a physical process of surface wave breaking, and surface roughness length.

From the idealized tests, we conclude that the modification of the Charnok parameter and the inclusion of the surface wave breaking are clearly the most relevant factors. Results from a realistic simulation in the Adriatic Sea during wind storm conditions are less straightforward to analyze, mainly because, contrary to the idealized test case, there are several aspects that can play a relevant role in the determination of the correct trajectories, including the accuracy of the wind forcing and the overall dynamics of the basin. We find that drifters' trajectories are better simulated when wave breaking processes are accounted for in the SOC models resolving the vertical mixing, provided the parameterization proposed in this paper adopts an enhanced coefficient α_{CH} with respect to the one originally proposed by Charnok (1955).

In agreement with what Stacey (1999), Stips et al. (2005) and Jones and Monismith (2008) also suggested, by employing a larger surface roughness with respect to that commonly used we are able to obtain a better agreement between simulated and real drifters' trajectories. More than that, we show that the determination of the surface roughness length seems to be the most critical model input parameter in controlling the correct prediction of the upper layer velocity in the ocean.

Both the determination of the surface roughness values in case of non-breaking waves and the large values adopted for it in case of breaking waves, are the subject of an active debate. Gemmrich and Farmer (1999), fitting data obtained via a freely drifting instrument, suggested a value of z_0 = 0.2 m, much less than values suggested in the literature by Craig (1996) or Terray et al. (1996). However, the authors pointed out how this value is actually heavily depending on choice of the empirical constant adopted in the turbulence models. Again Gemmrich and Farmer (2004), analyzing a dataset acquired through a surface-following float tethered to a vessel, provided indications on how the turbulence models origin can play a relevant role in reproducing observed values of dissipation, showing a comparison between the Craig and Banner (1994) and the Umlauf and Burchard (2003) approaches, the latter being the model at the basis of this paper.

As outlined in the statistical assessment section, the relative interplay between different combinations of schemes/parameters generates errors in the results in the range of 25–50% with respect to the total distance traveled daily by the satellite-tracked drifters. This suggests that selecting one configuration among others does matter.

This paper presents only some of the most relevant oceanographic aspects related to the surface drift modeling. Results show that, to some of these issues, interesting and successful suggestions recently formulated can be promptly implemented into state-of-the-art numerical tools. As a further suggestion, we believe that in order to successfully model the realistic nonlinear interactions among currents, wind and waves, there arises the necessity of modeling the atmospheric and oceanic systems as a coupled one. In many other cases, such as the influence of air bubbles on mixing, the influence of high-frequency meteorological input, the presence of non-local terms into vertical mixing schemes and the capability of wind models to capture gustiness, ongoing research activity is still seeking more satisfying explanations and successful implementations.

Acknowledgements

This work was sponsored by VECTOR-FISR Project and partially by the Office of Naval Research (ONR) under Grant number N00014-05-1-0730. The partial support from the Research Contract between CNR-ISMAR and ARPA-SIMC and the CMCC is also grateful acknowledged. Drifters data were made available thanks to P.-M. Poulain (OGS Trieste, Italy) and NURC Italy. ARPA-SIM in Bologna is acknowledged for providing us with LAMI and Po river discharges data during the framework of the NURC project ADRIA02-ADRIA03. We thank the ROMS and GOTM team for making the Regional Ocean Modeling System and the General Ocean Turbulence Model available to the scientific world as community models. Last, the authors are thankful to Prof. V.M. Canuto, to an anonymous reviewer and to the Journal Editor who greatly improved the quality of the manuscript.

References

Askari, F., Signell, R.P., Chiggiato, J., Doyle, J., 2003. RADARSAT mapping of Bora/Sirocco winds in the Adriatic Sea. In: Proceedings of IGARSS, 2003, IEEE International Geoscience and Remote Sensing Symposium, vol. 1, Toulouse, France, pp. 236–238.

Barron, C.N., Smedstad, L.F., Dastugue, J.M., Smedstad, O.M., 2007. Evaluation of ocean models using observed and simulated drifter trajectories: impact of sea surface height on synthetic profiles for data assimilation. J. Geophys. Res. 112, C07019. doi:10.1029/2006JC003982.

Beg-Paklar, G., Zagar, N., Zagar, M., Vellore, R., Koracin, D., Poualin, P.-M., Orlic, M., Vilibic, I., Dadic, V., 2008. Modeling the trajectories of satellite-tracked drifters in the Adriatic Sea during a summertime Bora event. J. Geophys. Res. 113, C11S04. doi:10.1029/2007JC004536.

Bignami, F., Sciarra, R., Carniel, S., Santoleri, R., 2007. The variability of the Adriatic Sea coastal turbid waters from SeaWiFS imagery. J. Geophys. Res. 112, C03S10. doi:10.1029/2006JC003518.

Booij, N., Ris, R.C., Holthuijsen, L.H., 1999. A third-generation wave model for coastal regions. Part I. Model description and validation. J. Geophys. Res. C4, 7649–7666.

Budyko, K., 1974. Climate and Life. Academic Press. 508 pp.

Breivik, O., Allen, A., 2008. An operational search and rescue model for the Norwegian Sea and the North Sea. Journal of Marine Systems 69 (1–2), 99–113.

Breivik, O., Saetra, O., 2001. Real time assimilation of HF radar currents into a coastal ocean model. J. Mar. Syst. 28 (3–4), 161–182.

Burchard, H., 2001. Simulating the wave-enhanced layer under breaking surface waves with two-equation turbulence models. J. Phys. Oceanogr. 31, 3133–3145.

Burchard, H., Bolding, K., 2001. Comparative analysis of four second-moment turbulence closure models for the oceanic mixed layer. J. Phys. Oceanogr. 31, 1943–1968.

Canuto, V.M., Howard, A., Cheng, J., Dubovikov, M.S., 2001. Ocean turbulence. Part I. One-point closure model-momentum and heat vertical diffusivities. J. Phys. Oceanogr. 31 (6), 1413–1426.

Carniel, S., Umgiesser, G., Kantha, L.H., Monti, S., Sclavo, M., 2002. Tracking the drift of a human body in the coastal ocean using Numerical Prediction Models of the oceanic, atmospheric and wave conditions. Science & Justice 42 (3), 143–151.

Carniel, S., Vichi, M., Sclavo, M., 2007. Sensitivity of a coupled physical-biological model to turbulence: high frequency simulations in a northern Adriatic station. Chemistry and Ecology 23 (2), 157–175. doi:10.1080/02757540701197903.

Castellari, S., Griffa, A., Ozgokmen, T.M., Poulain, P.-M., 2001. Prediction of particle trajectories in the Adriatic Sea using Lagrangian data assimilation. J. Mar. Syst. 29, 33–50.

Charnok, H., 1955. Wind stress on a water surface. Quart. J. R. Meteorol. Soc. 81, 639–640.

Craig, P., 1996. Velocity profiles and surface roughness under breaking waves. J. Geophys. Res. 101, 1265–1277.

Craig, P., Banner, M., 1994. Modelling wave-enhanced turbulence in the ocean surface layer. J. Phys. Oceanogr. 24, 2546–2559.

Cushman-Roisin, B., Naimie, C.E., 2002. A 3D finite-element model of the Adriatic tides. J. Mar. Syst. 37, 279–297.

Dorman, C.E., Carniel, S., Cavaleri, L., Sclavo, M., Chiggiato, J., Doyle, J., Haack, T., Pullen, J., Grbec, B., Vilibić, I., Janeković, I., Lee, C., Malačič, V., Orlić, M., Paschini, E., Russo, A., Signell, R.P., 2006. February 2003 marine atmospheric conditions and the bora over the northern Adriatic. J. Geophys. Res. 111, C03S03. doi:10.1029/2005JC003134.

Fairall, C.W., Bradley, E.F., Hare, J.E., Grachev, A.A., Edson, J.B., 2003. Bulk parameterisations of air–sea fluxes: updates and verification for the COARE algorithm. J. Clim. 16, 571–591.

Galperin, B., Kantha, L.H., Hassid, S., Rosati, A., 1988. A quasi-equilibrium turbulent energy model for geophysical flows. J. Atmos. Sci. 45, 55–62.

Gemmrich, J.R., Farmer, D.M., 1999. Near-surface turbulence and thermal structure in a wind driven sea. J. Phys. Oceanogr. 29, 480–499.

Gemmrich, J.R., Farmer, D.M., 2004. Near-surface turbulence in the presence of breaking waves. J. Phys. Oceanogr. 34, 1067–1086.

Haidvogel, D.B., Arango, H., Budgell, W.P., Cornuelle, B.D., Curchitser, E., Di Lorenzo, E., Fennel, K., Geyer, W.R., Hermann, A.J., Lanerolle, L., Levin, J., McWilliams, J.C., Miller, A.J., Moore, A.M., Powell, T.M., Shchepetkin, A.F., Sherwood, C.R., Signell, R.P., Warner, J.C., Wilkin, J., 2008. Ocean forecasting in terrain-following coordinates: formulation and skill assessment of the Regional Ocean Modeling System. J. Comp. Phys. 227, 3595–3624.

Haza, A.C., Griffa, A., Martin, P., Molcard, A., Özgökmen, T.M., Poje, A.C., Barbanti, R., Book, J.W., Poulain, P.-M., Rixen, M., Zanasca, P., 2007. Model-based directed drifter launches in the Adriatic Sea: results from the DART experiment. Geophys. Res. Lett. 34, L10605. doi:10.1029/2007GL029634.

Jones, N.L., Monismith, S.G., 2008. Modeling the influence of wave-enhanced turbulence in a shallow tide- and wind-driven water column. J. Geophys. Res. 113, C03009. doi:10.1029/2007JC004246.

Kantha, L.H., 2006. Comments on "Second-order turbulence closure models for geophysical boundary layers. A review of recent work". Cont. Shelf Res. 26 (81), 9–822.

Kantha, L.H., Carniel, S., 2003. Comments on "A generic length-scale equation for geophysical turbulence models" by L. Umlauf and H. Burchard. J. Mar. Res. 61 (5), 693–702. doi:10.1357/002224003771816007.

Kantha, L.H., Clayson, C.A., 1994. An improved mixed layer model for geophysical applications. J. Geophys. Res. 99, 25235–25266.

Kantha, L.H., Clayson, C.A., 2004. On the effect of surface gravity waves on mixing in the oceanic mixed layer. Ocean Modell. 6, 101–124.

Kundu, P.K., 1976. Ekman veering observed near the ocean bottom. J. Phys. Oceanogr. 6, 238–242.

Kuzmić, M., Janeković, I., Book, J.W., Martin, P.J., Doyle, J.D., 2006. Modeling the northern Adriatic double-gyre response to intense bora wind: a revisit. J. Geophys. Res. 111, C03S13. doi:10.1029/2005JC003377 [printed 112(C3), 2007].

Lee, C. et al., 2005. Northern Adriatic response to a wintertime bora wind event. Eos Trans. AGU 86 (16), 157. 163, 165.

Margolin, L., Smolarkiewicz, P.K., 1998. Antidiffusive velocities for multipass donor cell advection. SIAM J. Sci. Comput. 90, 7–929.

Martin, P.J., Book, J.W., Doyle, J.D., 2006. Simulation of the northern Adriatic circulation during winter 2003. J. Geophys. Res. 111, C03S12. doi:10.1029/2006JC003511 [printed 112(C3), 2007].

Mellor, G.L., Yamada, T., 1982. Development of a turbulence closure model for geophysical fluid problems. Reviews of Geophysics and Space Physics 20, 851–875.

Orlić, M., Kuzmić, M., Pasarić, Z., 1994. Response of the Adriatic Sea to the bora and sirocco forcing. Cont. Shelf Res. 14, 91–116.

Ozgokmen, T.M., Piterbarg, L.I., Mariano, A.J., Ryan, E.H., 2001. Predictability of drifter trajectories in the tropical Pacific Ocean. J. Phys. Oceanogr. 31, 2691–2720.

Poulain, P.-M., 2001. Adriatic Sea surface circulation as derived from drifter data between 1990 and 1999. Journal of Marine Systems 29 (1–4), 3–32.

Poulain, P.-M., Gerin, R., Mauri, E., Pennel, R., 2009. Wind effects on drogued and undrogued drifters in the Eastern Mediterranean. J. Atm. Oc. Tech. doi:10.1175/2008JTECH0618.1.

Pullen, J., Doyle, J.D., Haack, T., Dorman, C., Signell, R.P., Lee, C.M., 2007. Bora event variability and the role of air–sea feedback. J. Geophys. Res. 112, C03S18. doi:10.1029/2006JC003726.

Reed, M., Johansen, O., Brandvik, P.J., Daling, P., Lewis, A., Fiocco, R., Mackay, D., Prentki, R., 1999. Oil spill modeling towards the close of the 20th century: overview of the state of the art. Spill Science and Technology Bulletin 5 (1), 3–16.

Rixen, M., Ferreira-Coelho, E., Signell, R.P., 2007. Surface drift prediction in the Adriatic Sea using hyper-ensemble statistics on atmosphere, ocean and wave models: uncertainties and probability distribution areas. J. Mar. Syst. 69 (1–2), 86–98. doi:10.1016/j.marsys.2007.02.015.

Rodi, W., 1987. Examples of calculation methods for flow and mixing in stratified fluids. J. Geophys. Res. 92, 5305–5328.

Shchepetkin, A.F., McWilliams, J.C., 1998. Quasi-monotone advection schemes based on explicit locally adaptive dissipation. Monthly Weather Review 126, 1541–1580.

Shchepetkin, A.F., McWilliams, J.C., 2003. A method for computing horizontal pressure-gradient force in an oceanic model with a non-aligned vertical coordinate. J. Geophys. Res. 108 (C3), 3090. doi:10.1029/2001JC001047.

Shchepetkin, A.F., McWilliams, J.C., 2005. The regional ocean modelling system: a split-explicit, free-surface, topography-following-coordinates ocean model. Ocean Modell. 9, 347–404.

Sherwood, C.R., Carniel, S., Cavaleri, L., Chiggiato, J., Das, H., Doyle, J.D., Harris, C.K., Niedoroda, A.W., Pullen, J., Reed, C.W., Russo, A., Sclavo, M., Signell, R.P., Traykovski, P., Warner, J.C., 2004. Sediment dynamics in the Adriatic Sea investigated with coupled models. Oceanography 17 (4), 46–57.

Signell, R.P., Carniel, S., Terray, E.A., Burchard, H., 2002. The effect of wind wave breaking and vertical resolution on simulation of surface currents in 3D hydrodynamical models. Eos Trans. AGU 83 (4), Ocean Sci. Meet. Suppl., Abstract OS42B-134, Hawaii, USA.

Signell, R.P., Carniel, S., Cavaleri, L., Chiggiato, J., Doyle, J., Pullen, J., Sclavo, M., 2005. Assessment of wind quality for oceanographic modeling in semi-enclosed basins. J. Mar. Syst. 53 (1–4), 217–233. doi:10.1016/j.marsys.2004.03.006.

Song, Y., Haidvogel, D.B., 1994. A semi-implicit ocean circulation model using a generalized topography-following coordinate system. J. Comp. Phys. 115 (1), 228–244.

Stacey, M.W., 1999. Simulation of the wind-forced near-surface circulation in knight inlet: a parameterization of the roughness length. J. Phys. Oceanogr. 29, 1363–1367.

Steppeler, J., Doms, G., Shatter, U., Bitzer, H.W., Gassmann, A., Damrath, U., Gregoric, G., 2003. Meso-gamma scale forecasts using the nonhydrostatic model LM. Meteorol. Atmos. Phys. 82, 75–96.

Stips, A., Burchard, H., Bolding, K., Prandke, H., Simon, A., Wuest, A., 2005. Measurement and simulation of viscous dissipation in the wave affected surface layer. Deep Sea Res. II 52, 1133–1155.

Taillandier, V., Griffa, A., Poulain, P.M., Signell, R.P., Chiggiato, J., Carniel, S., 2008. Variational analysis of drifter positions and model outputs for the reconstruction of surface currents in the Central Adriatic during fall 2002. J. Geophys. Res. 35, L02605. doi:10.1029/2007JC004148.

Terray, E., Donelan, M., Agarwal, Y., Drennan, W., Kahma, K., Williams III, A.J., Hwang, P., Kitaigorodskii, S.A., 1996. Estimates of kinetic energy dissipation under breaking waves. J. Phys. Oceanogr. 26, 972–987.

Umlauf, L., Burchard, H., 2003. A generic length-scale equation for geophysical turbulence. J. Mar. Res. 61, 235–265.

Umlauf, L., Burchard, H., 2005. Second-order turbulence closure models for geophysical boundary layers. A review of recent work. Cont. Shelf Res. 25, 795–827.

Umlauf, L., Burchard, H., Hutter, K., 2003. Extending the k-ω model towards oceanic applications. Ocean Modell. 5, 195–218.

Ursella, L., Poulain, P.-M., Signell, R.P., 2006. Surface drifter derived circulation in the northern and middle Adriatic Sea: response to wind regime and season. J. Geophys. Res. 111, C03S04. doi:10.1029/2005JC003177.

Warner, J.C., Sherwood, C.R., Arango, H.G., Signell, R.P., 2005. Performance of four turbulence closure models implemented using a generic length scale method. Ocean Modell. 8, 81–113.

Wilcox, D., 1988. Reassessment of the scale-determining equation for advanced turbulence models. AIAA J. 26, 1299–1310.
Wilcox, D., 1998. Turbulence modeling for CFD. DCW Industries, second ed. La Cañada, California, p. 540.
Zoubir, A.M., 1993. Bootstrap: theory and applications. In: Luk, T. (Ed.), Proceedings of SPIE, Advanced Signal Processing Algorithms, Architectures and Implementations, vol. 2027, San Diego, pp. 216–235.